ISSN 0003-701X, Applied Solar Energy, 2021, Vol. 57, No. 2, pp. 113–119. © Allerton Press, Inc., 2021.
Russian Text © The Author(s), 2021, published in Geliotekhnika, 2021, No. 2, pp. 151–157.

SOLAR ENGINEERING
MATERIALS SCIENCE

Surface Morphology and Phase Composition of (Zn,Sn)Se Thin Films, Obtained by Chemical-Molecular Beam Deposition

T. M. Razykov[a], K. M. Kuchkarov[a, *], M. S. Tivanov[b, **], D. S. Bayko[b], I. A. Kaputskaya[b], N. I. Poliak[b], O. V. Korolik[b], B. A. Ergashev[a], R. T. Yuldoshov[a], R. R. Khurramov[a], J. Bekmirzaev[a], A. Olimov[a], D. Isakov[a], M. Makhmudov[a], and M. Pirimmatov[a]

[a] *Physical–technical Institute SPA "Physics–Sun," AS RUz, Tashkent, 100084 Uzbekistan*
[b] *Faculty of Physics, Belarusian State University, Minsk, 220030 Belarus*
**e-mail: k.kuchkarov@mail.ru*
***e-mail: michael.tivanov@gmail.com*

Received July 10, 2020; revised August 14, 2021; accepted September 4, 2021

Abstract—(Zn,Sn)Se films of different chemical composition ratio Zn/Sn were obtained by chemical molecular beam deposition (CMBD) method on borasilicate glass with variation the ratio of the partial pressure of ZnSe and SnSe in vapour phase during growth. Chemical and phase composition, as well as surface morphology of samples were investigated. The samples were found to be a thin films with a thickness of 2–3 μm with and evenly distribution of chemical elements. Grain structure, phase composition and surface roughness parameters dependencies on the elemental composition are determined.

Keywords: chemical molecular beam deposition (CMBD), (Zn,Sn)Se , morphology, structure, Raman scattering

DOI: 10.3103/S0003701X21020092

INTRODUCTION

Recently, silicon with an efficiency of 27.6%, $Cu(In,Ga)Se_2$ – 23.35% and CdTe – 22.1% are the leading materials on the world market of photovoltaics [1]. Despite the wide application of the mentioned materials, there are significant limitations on their applying in the global production of photovoltaic modules. The main disadvantages of Si use as a base material for solar cells are: the band gap of silicon (1.1 eV) is less, than the optimal value of 1.4–1.6 eV [2], the absorption coefficient is low (~10^2 cm^{-1}). Therefore, it is necessary to use a material with a higher thickness (100–200 μm), which cause the increase in the cost of the final product [3]. At the same time, further widespread use of thin-film solar cells based on $Cu(In,Ga)Se_2$ and CdTe causes great difficulties, because of the limited reserves of In, Ga, Te in the earth's crust, and the toxicity of cadmium [4].

Considering this, many scientific groups concentrate their research work to replace the above-mentioned expensive In and Ga materials with Zn and Sn [5]. The optical properties of metal chalcogenides on Zn and Sn base are similar to the properties of $Cu(In,Ga)Se_2$ [6]. At the same time, the advantages are their low cost (large reserves in nature) and non-toxicity. At present, the efficiency of solar cells based on $Cu_2ZnSn(S,Se)_4$ is 12.6%. This efficiency was obtained at the IBM Research Center and is the maximum value over the past 20 years [7]. However, this value is much lower, than efficiency of solar cells based on $Cu(In,Ga)Se_2$, that reaches the value 19.8–20.3% [8, 9]. According to the investigations, such low efficiency is caused by the complexity of methods for obtaining and controlling the composition of films [10].

The mentioned disadvantages can be overcome by replacing the absorber with a new material, possessing the following characteristics: first of all, the new material must be inexpensive, non-toxic, and widespread in the earth's crust; secondly, this material should have an optimal band gap, a high absorption coefficient and a low recombination rate, to provide a high diffusion length of charge carriers.

(Zn,Sn)Se has no disadvantages found in Si, $Cu(In,Ga)Se_2$ and CdTe. This material has unique properties for creating thin-film solar cells: high absorption coefficient ~10^5 cm^{-1}, optimal band gap ~1.45 eV, *p*-type of conductivity; besides, Zn, Sn, Se are cheap and widespread in the earth's crust [11].

In this work, investigated the surface morphology and phase composition of a new material (Zn,Sn)Se (ZTSe) with various chemical compositions, obtained by chemical molecular beam deposition (CMBD), at a substrate temperature of 550ºC, have been considered.

Table 1. Chemical composition of the studied films

Sample	Atomic percentage (%)			Atomic ratio	
	Zn	Sn	Se	Zn/(Sn + Zn)	metal/chalcogen
Sample 1 ($x = 0.02$)	1.0	46.0	53.0	0.021	0.887
Sample 2 ($x = 0.06$)	3.2	47.6	49.2	0.063	1.033
Sample 3 ($x = 0.10$)	5.3	45.9	48.8	0.104	1.049
Sample 4 ($x = 0.20$)	10.0	40.1	49.9	0.200	1.004

EXPERIMENTAL DETAILS

Film preparation. The preparation of ZTSe films by the CMBD method is described in detail in [12]. SnSe and ZnSe powders of semiconductor purity (99.999%) were used as precursors, which were evaporated in a hydrogen flow at atmospheric pressure. The evaporation temperature of SnSe and ZnSe powders for film grows was in the range 820–860 and 910–920°C, respectively, the substrate temperature was 550°C. The flow of hydrogen carrier gas was ~20 cm^3/min.

The duration of the deposition process was in the range from 30 to 60 min. Borasilicate glasses ($B_2O_3 + SiO_2$) were used as substrates. The composition of the obtained ZTSe films was changed by controlling the ratio of the partial pressure of ZnSe and SnSe in the vapor phase, during the growth process.

Characterization techniques. The surface morphology of the films was investigated, by using a S-806 (Hitachi) scanning electron microscope (SEM). The chemical composition was determined by energy dispersive X-ray (EDX) analysis, using a CAMECA SX-100.

The structural characteristics of the samples were analyzed, by using an Ultima IV (Rigaku) X-ray diffractometer in the grazing incidence diffraction geometry (GIXD) at 1 degree of incident X-rays with CuK_α radiation source (λ = 1.54178 Å). XRD analysis was carried out with the use of the database of the Joint Committee on Powder Diffraction Standard (JCPDS) and Crystallography Open Database (COD).

Raman spectra were measured at room temperature, using a Nanofinder HE confocal spectrometer (LOTIS TII). A solid-state laser (radiation wavelength is 532 nm) was used to excite. The power of laser radiation incident on the samples was reduced to 60 μW, to avoid their thermal damage. Spectral resolution was better, than 2.5 cm^{-1}. The size of the area, on which the laser radiation was focused on the surface of the samples, was about 0.7 μm in diameter.

The surface topography of the films was analyzed, using a Solver Nano (NT-MDT) atomic force microscope (AFM). The AFM instrument was used in the semi-contact mode, with a scanning probe of 10 nm tip radius, at a resonance frequency of 236 kHz.

RESULTS AND DISCUSSION

The results of the EDX analysis (tab. 1) show, that the deposited (Zn,Sn)Se films have a different composition $x = Zn/(Sn + Zn)$ ($x = 0.02, 0.06, 0.10, 0.20$). It should be noted, that the most stoichiometric composition, in terms of the metal/chalcogen ratio, is obtained for the film with the highest Zn content ($x = 0.20$).

ZTSe films, obtained by the CMBD method, were appeared to be grey in colour, uniform, pinhole free and were well adherent to the substrate surface, and their thickness was about 2–3 μm (Fig. 1).

Figures 2a–2d show the 2D SEM pictures of the samples surface. The obtained films mainly consist from individual densely spaced grains (light areas) on glass substrate (dark areas). Significant differences of

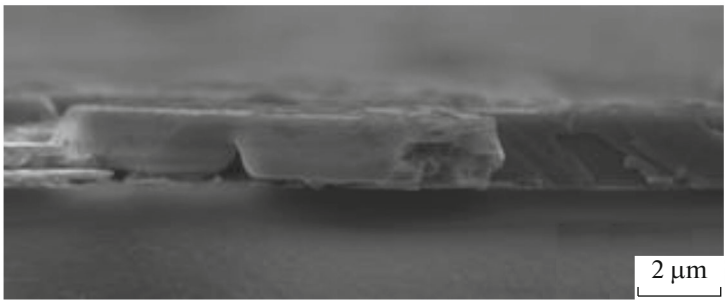

Fig. 1. Typical SEM cross-section view of the ZTSe films.

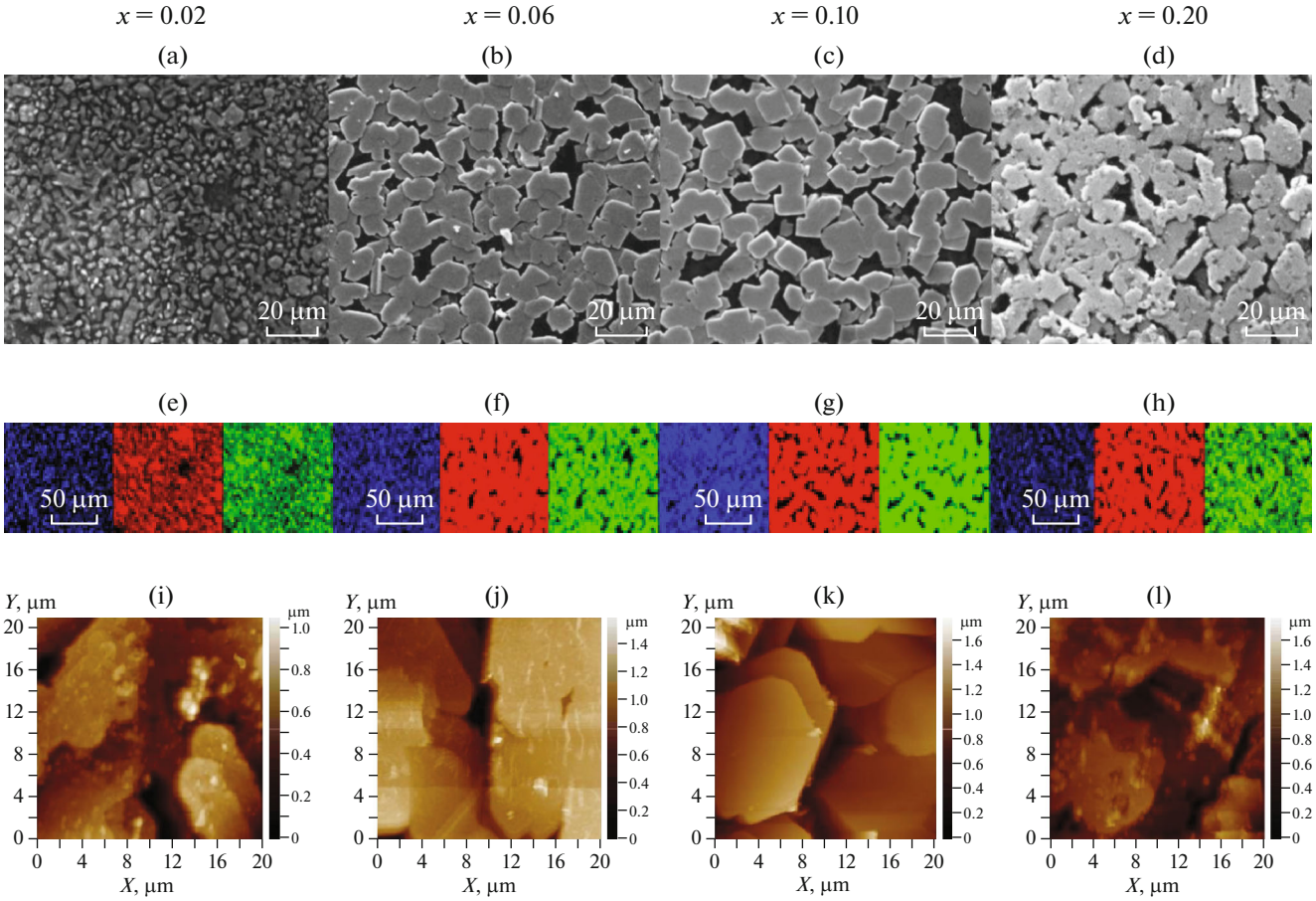

Fig. 2. SEM Surface morphology (a–d), EDX surface arrangement of elements (e–h) and AFM topography of the (Zn,Sn)Se films: ■—Zn, ■—Sn, ■—Se.

the surface morphology, associated with the difference of composition ratio *x,* were found. Grains of the samples with $x = 0.02$ are located in islands on glass substrate and have the form of drops, with an average size of 5 μm (Fig. 2a). With the increase of *x,* the grains forms flattened, layered clusters with near equiaxial shapes, moreover for $x = 0.06$ and $x = 0.10$, the grains have a faceting (Figs. 2b, 2c). The faceting is more distinct for $x = 0.10$, but it decreases for $x = 0.20$, while uneven graininess, with the size of 10–20 μm, is appeared, the grains partially acquire elongated form (Fig. 2d).

X-ray spectral microanalysis shows, that the chemical elements Se, Sn, Zn, which form the films, are evenly distributed (Figs. 2e–2h). This is a positive effect of CMBD since a uniform distribution of chemical elements in the samples determines the uniformity of their phase composition. Such films possess the required properties, and it becomes possible to change the properties in the desired functional range, by changing the content of elements.

AFM investigation of films reveals, that the average surface roughness and root mean square roughness increases, with an increase of *x* (see Figs. 2i–2l and Table 2). The sample with the clearest faceting ($x = 0.10$) is characterized by the highest surface roughness, which is 1.7 times higher, than that of the sample with drop-shaped grains. A decrease in the roughness of the sample with $x = 0.20$ confirms the loss of faceting of grains and the appearance of uneven graininess, observed in the SEM images.

It is found , that the skewness of the distribution of peaks in the films is negative and varies in the range from –1.10 to –0.4, with an increase in the parameter *x*, which indicates, that the distribution of heights tends to normal, with an increase in x and, at a maximum $x = 0.20$, almost coincides with it. This implies a transition from a slightly asymmetric distribution of heights to a symmetric distribution at higher *x* values [13]. In addition, it was found, that the kurtosis values are >3, which indicates a smaller height spread, than for the normal distribution [13]. Analysis of phase diagrams of Sn–Se, Se–Zn, Sn–Zn systems [13, 14] shows, that mainly phases of $SnSe_2$, SnSe, Se, Sn, β–Sn are forming in the ZTSe and in less extent phase of ZnSe.

Table 2. Surface roughness parameters of (Zn,Sn)Se thin films

Zn/(Sn + Zn)	Arithmetic average height Sy, μm	Average roughness Ra, nm	Root mean square roughness Rrms, nm	Skewness Rsk	Kurtosis Rku
$x = 0.02$	1.12	95	127	–0.88	5.56
$x = 0.06$	1.65	130	185	–1.10	6.4
$x = 0.10$	1.74	170	220	–0.23	3.37
$x = 0.20$	1.33	130	169	–0.4	3.73

X-ray diffraction analysis was carried out to determine the phase composition of ZTSe films, the results are presented in Fig. 3.

The X-ray analysis method used of obtained GIXD patterns is based on search of coincidence of the experimental values of the interplanar distances d_{exp} and intensities I_{exp} of diffraction lines with the corresponding values d_{cat} and I_{cat} of diffraction patterns of probable compounds from data catalogs. This analysis makes it possible to conclude about the presence or absence of the corresponding phase in the sample.

Analyzing the ratio of the integrated intensities of these phases (I, %), it can be suggested, that the films mainly consist of $SnSe_2$ and SnSe, to a lesser extent of Se (Table 3). With the increase of x from 0.02 to 0.06, 0.10, 0.20, stoichiometric composition the diffraction patterns show a redistribution of the integral intensities of the reflections of $SnSe_2$ and SnSe phases, decrease of most reflections of Se and SnSe phases intensity up to their disappearance, emergence of ZnSe phase weak reflections at $x = 0.20$. There is a noticeable increase in the relative intensity of the reflex at $2\theta = 52.65°$, which can be corresponding to crystallographic orientation (103) of $SnSe_2$ phase or to crystallographic orientation (610) of SnSe phase.

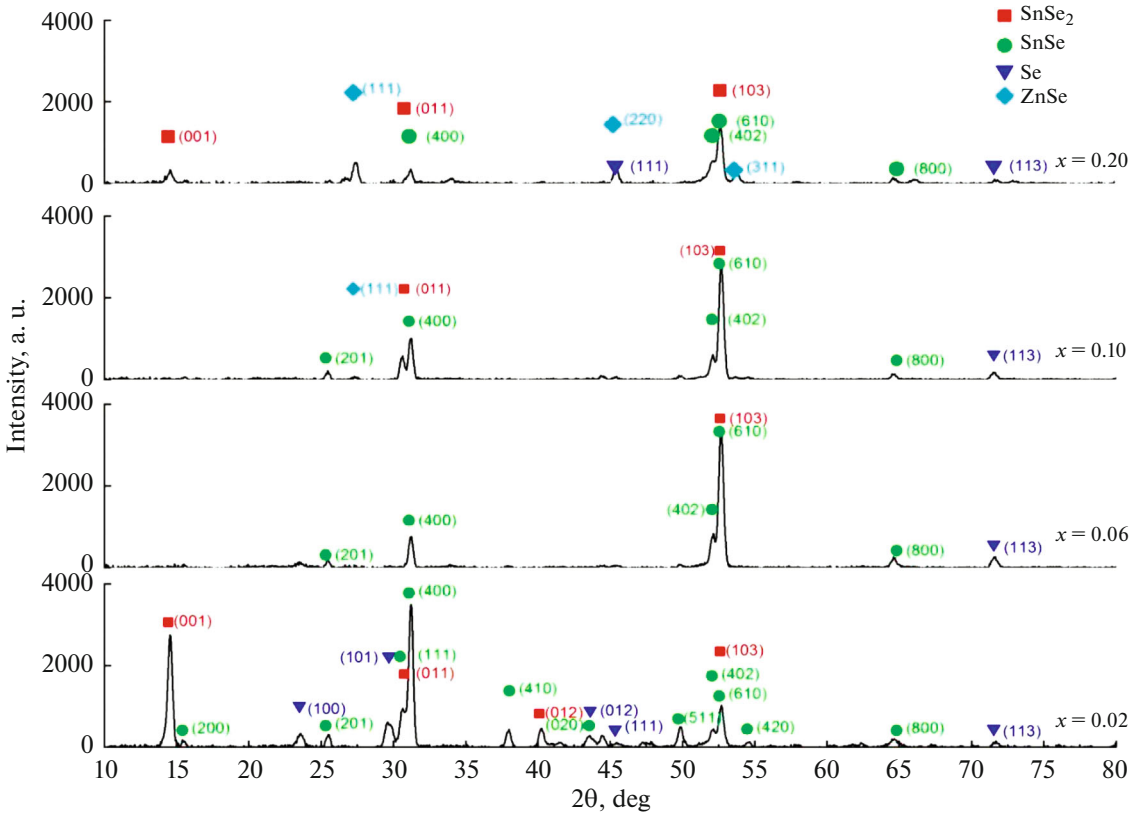

Fig. 3. GIXD patterns of ZTSe films.

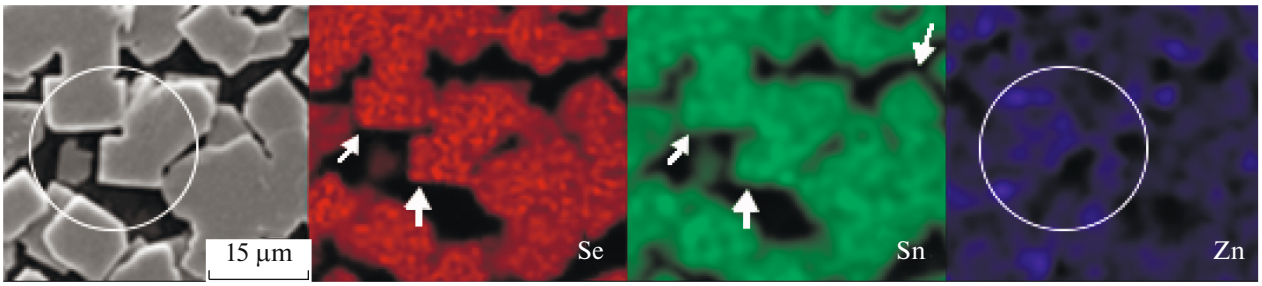

Fig. 4. The faceting of grains in sample with $x = 0.10$.

RESULTS OF INDEXING REFLECTIONS IN DIFFRACTOGRAMS

$SnSe_2$					SnSe					Se					ZnSe				
	I_{HKL}, %					I_{HKL}, %					I_{HKL}, %					I_{HKL}, %			
HKL	*x*				*HKL*	*x*				*HKL*	*x*				*HKL*	*x*			
	0.02	0.06	0.10	0.20		0.02	0.06	0.10	0.20		0.02	0.06	0.10	0.20		0.02	0.06	0.10	0.20
001	80	–	20	23	200	5	–	–	–	100	10	–	–	–	111	–	–	3	35
011	78	–	30	24	201	9	4	7	–	101	18	–	–	–	220	–	–	–	24
012	13	–	–	–	111	27	–	–	–	012	8	–	–	–	311	–	–	–	17
103	30	*100*	*100*	*100*	400	*100*	22	36	24	111	3	–	–	24					
					410	12	–	–	–	113	3	9	6	7					
					020	9	–	–	–										
					511	14	–	–	–										
					402	11	22	22	37										
					610	29	*100*	*100*	*100*										
					420	4	–	–	–										
					800	6	8	5	–										

The faceting of grains in samples with $x = 0.06$, 0.10 and 0.20, detected by SEM (Figs. 2b–2d), also indirectly confirms, that the grains consist mainly of $SnSe_2$ (Table 3), which has a hexagonal lattice. Also, a layered grain structure is found for such a film compositions (Figs. 2b–2d). A similar layered structure of $SnSe_2$ and SnSe is reported in [15]. It should be noted, that especially for these compositions, preferential orientation of $SnSe_2$ grains appears and this can indicate the presence of texture (103) (Table 3, Fig. 4). It can be seen from the EDX analysis (Fig. 4), that Se and Sn, which are part of the grains, repeat their outlines, while Zn is located in separate areas, possibly in the form of clusters.

The XRD pattern of films with small *x* doesn't confirm the presence of a significant amount of ZnSe or ZnSn phases. The XRD pattern of the film with $x = 0.20$ includes lines, which can probably be attributed to ZnSe (Fig. 3). To clarify this assumption, the samples were studied using Raman spectroscopy.

Raman experiment on the films allows to distinguish two types of areas with different typical Raman spectra—type I and type II (see inserts on Fig. 5). With an increase in *x*, the type I areas increase and the type II areas decrease. Figure 5 shows the Raman spectra of films with minimum and maximum values of *x*: $x = 0.02$ (sample 1) and $x = 0.2$ (sample 4).

For sample 1 ($x = 0.02$), lines specific to α-SnSe (70–75, 108–110, 130–133, 150, 185–187 cm^{-1}) are defined in the I type areas [16]. Some low-intensity lines are observed in the region of 235 and 254 cm^{-1}, the 235 cm^{-1} line can be attributed to Se, with a trigonal structure [16, 17], the 254 cm^{-1} line can be attributed to amorphous Se [16, 17]. In regions of type II, lines at 117 and 185 cm^{-1} are observed, and the line at 185 cm^{-1} is more intense, which is characteristic of $SnSe_2$ [16]. The high intensities of the lines at 235 and 143 cm^{-1} indicate, that Se with a trigonal structure may still be present [17] (the peak at 143 cm^{-1} is too narrow to correspond to 2TA phonon scattering in ZnSe).

For sample 4 with $x = 0.20$, lines characteristic to α-SnSe are defined in the I type areas, also (70–75,

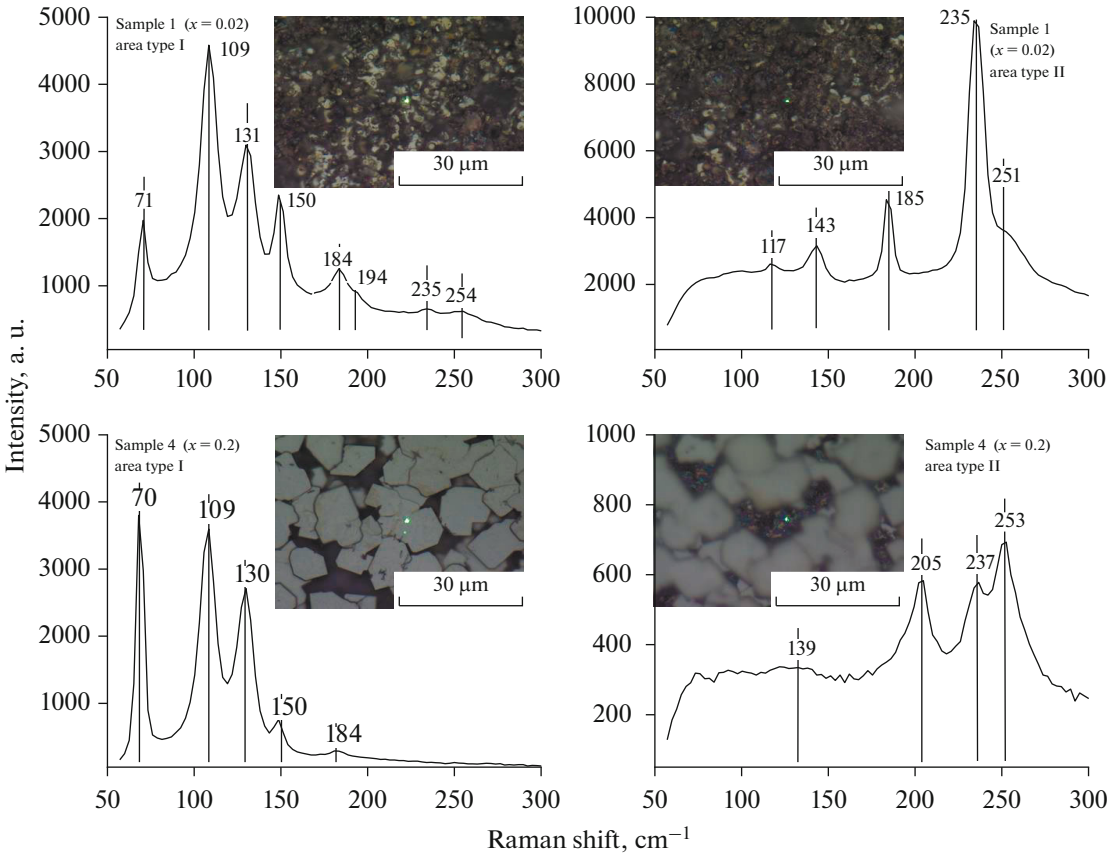

Fig. 5. Raman spectra of (Zn,Sn)Se films.

108–110, 130–133, 150, 185–187 cm^{-1}). Broad lines are observed in the range of 139, 205, 237 and 253 cm^{-1} in the II type areas [18, 19]. These lines correspond to ZnSe (line at 205 cm^{-1} can be attributed to TO phonon, line at 237 cm^{-1} corresponds to surface phonons of ZnSe nanoparticles, line at 253 cm^{-1} can be attributed to LO phonon, line at 139 cm^{-1} can be attributed to the 2TA phonon) [17, 18].

CONCLUSIONS

In conclusion, the structure, morphology and Raman scattering characteristics of the (Zn,Sn)Se films were investigated by GIXD, SEM, AFM, and Raman spectra. The results presented in this work can besummarised as follows:

1. Analyzing the ratio of the integrated intensities of the phases (I, %), it can be suggested, that the films mainly consist of $SnSe_2$ and SnSe, to a lesser extent of Se. With the increase of x from 0.02 to 0.06, 0.10, 0.20, stoichiometric composition the diffraction patterns show a redistribution of the integral intensities of the reflections of $SnSe_2$ and SnSe phases, decrease of most reflections of Se and SnSe phases intensity up to their disappearance, emergence of ZnSe phase weak reflections at $x = 0.20$.

2. Significant differences of the surface morphology, associated with the difference of composition ratio x, were found Grains of the samples with $x = 0.02$ are located in islands on glass substrate and have the form of drops, with an average size of 5 μm. With the increase of x, the grains forms flattened, layered clusters with near equiaxial shapes, moreover for $x = 0.06$ and $x = 0.10$, the grains have a faceting.

3. AFM investigation of films reveals, that the average surface roughness and root mean square roughness increases, with an increase of x.

Raman experiment on the (Zn,Sn)Se films allows to distinguish two types of areas with different typical Raman spectra – type I and type II. With an increase in x, the type I areas increase and the type II areas decrease. The Raman spectra of films with minimum and maximum values of x: $x = 0.02$ and $x = 0.2$.

FUNDING

This work is supported by the FA-F3-003 project at the Uz AS Physical–Technical Institute and by the Belarusian State Programme for Research "Materials science, new materials and technologies."

REFERENCES

1. Green, M., et al., Solar cell efficiency tables (version 53), *Prog. Photovoltaics,* 2019, vol. 27, no. 1, pp. 3–12.
2. Rühle, S., Tabulated values of the Shockley–Queisser limit for single junction solar cells, *Sol. Energy,* 2016, vol. 130, pp. 139–147. https://doi.org/10.1016/j.solener.2016.02.015
3. Razykov, T.M., Ferekides, C.S., et al., Solar photovoltaic electricity: Current status and future prospects, *Sol. Energy,* 2011, vol. 85, pp. 1580–1608.
4. Dhere, N.G., Scale-up issues of CIGS thin film PV modules, *Sol. Energy Mater. Sol. Cells,* 2011, vol. 95, no. 1, pp. 277–280.
5. Cao Yun, Wang Chunrui, Li Bin, et al., Fabrication and characterization of $Cu_2ZnSnS_xSe_{4-x}$ solid solution nanocrystallines, *Jpn. J. Appl. Phys.,* 2011, vol. 50, art. id. 125001. https://doi.org/10.1143/JJAP.50.125001
6. Stanley, M., Jubault, M., Donsanti, F., and Naghavi, N., Flexible $Cu(In,Ga)Se_2$ based solar cells using molybdenum foils as substrate, *Phys. Status Solidi,* 2017, vol. 14, no. 10, art. id. 1700174.
7. Wang, W., Winkler, M.T., Gunawan, O., et al., Characteristics of CZTSSe thin-film solar cells with 12.6% efficiency, *Adv. Energy Mater.,* 2013, vol. 4, no. 7, art. id. 1301465. https://doi.org/10.1002/aenm.201301465
8. Jackson, P., Hariskos, D., Lotter, E., et al., New world record efficiency for $Cu(In,Ga)Se_2$ thin film solar cells beyond 20%, *Prog. Photovoltaics Appl. Res.,* 2011, vol. 19, pp. 894–897.
9. Green, M.A., Emery, K., Hishikawa, Y., et al., Solar cells efficiency tables (version 43), *Prog. Photovoltaics Appl. Res.,* 2014, vol. 22, pp. 1–9.
10. Todorov, T.K., Tang, J., et al., Beyond 11% efficiency: Characteristics of state-of-the-art $Cu_2ZnSn(S,Se)_4$ solar cells, *Adv. Energy Mater.,* 2013, vol. 3, pp. 34–38.
11. Orletskyi, I.G., Solovan, M.M., Brus, V.V., et al., Structural, optical and electrical properties of Cu_2ZnSnS_4 films prepared from a non-toxic DMSO-based sol-gel and synthesized in low vacuum, *J. Phys. Chem. Solids,* 2017, vol. 100, pp. 154–160.
12. Razykov, T.M., Bosio, A., Ergashev, B., et al., Growth and characterization of $Zn_xSn_{1-x}Se$ films for use in thin film solar cells, *Sol. Energy,* 2019, vol. 193, pp. 519–522.
13. Moser, Z., Dutkiewicz, J., Gasior, W., and Salawa, J., The Sn–Zn (Tin–Zinc) system, *Bull. Alloy Phase Diagrams,* 1985, vol. 4, pp. 330–334, https://doi.org/10.1007/bf02880511
14. *Diagrammy sostoyaniya dvoynykh metallicheskikh sistem. Spravochnik (Phase Diagrams of Double Metallic Systems. Handbook)*, Lyakishev, N.P., Ed., Moscow: Mashinostroyeniye, 1996.
15. Narro-Rios, J.S., Ramachandran, M., Martínez-Escobar, D., and Sánchez-Juárez, A, Ultrasonic spray pyrolysis deposition of SnSe and $SnSe_2$ using a single spray solution, *J. Semicond.,* 2013. vol. 34, no. 1, art. id. 013001.
16. Salome, P.M.P., Fernandes, P.A., et al., Secondary crystalline phases identification in $Cu_2ZnSnSe_4$ thin films: Contributions from Raman scattering and photoluminescence, *Mater. Sci.,* 2014, vol. 49, pp. 7425–7436, https://doi.org/10.1007/s10853-014-8446-2
17. Pinto, A.H., Leite, E.R., Longo, E., and de Camargo, E.R., Crystallization at room temperature from amorphous to trigonal selenium as a byproduct of the synthesis of water dispersible zinc selenide, *Mater. Lett.,* 2012, vol. 87, no, 15, pp. 62–65, https://doi.org/10.1007/s10853-014-8446-2
18. Irmer, G., Monaico, E., Tiginyanu, I.M., et al., Frohlich vibrational modes in porous ZnSe studied by Raman scattering and Fourier transform infrared reflectance, *J. Phys. D: Appl. Phys.,* 2009, vol. 42, art. id. 045405.
19. Jing Xu, Aijiang Lu, Chunrui Wang, et al., ZnSe-based longitudinal twinning nanowires, *Adv. Eng. Mater.,* 2014, vol. 16, no. 4, pp. 459–465. https://doi.org/10.1002/adem.201300405